Published in final edited form as:
Neuroimage. 2009 April 1; 45(2): 614–626. doi:10.1016/j.neuroimage.2008.11.030.

Functional Connectivity of the Human Amygdala using Resting State fMRI

Amy Krain Roy[1], **Zarrar Shehzad**[1], **Daniel S. Margulies**[4], **A.M. Clare Kelly**[1], **Lucina Q. Uddin**[1], **Kristin Gotimer**[1], **Bharat B. Biswal**[2], **F. Xavier Castellanos**[1,3], and **Michael P. Milham**[1]

[1] Phyllis Green and Randolph C wen Institute for Pediatric Neuroscience, NYU Child Study Center

[2] Department of Radiology, University of Medicine and Dentistry of New Jersey

[3] Nathan Kline Institute for Psychiatric Research

[4] Berlin Institute for Mind and Brain, Humboldt Universitat, Berlin, Germany

Abstract

The amygdala is composed of structurally and functionally distinct nuclei that contribute to the processing of emotion through interactions with other subcortical and cortical structures. While these circuits have been studied extensively in animals, human neuroimaging investigations of amygdala-based networks have typically considered the amygdala as a single structure, which likely masks contributions of individual amygdala subdivisions. The present study uses resting state functional magnetic resonance imaging (fMRI) to test whether distinct functional connectivity patterns, like those observed in animal studies, can be detected across three amygdala subdivisions: laterobasal, centromedial, and superficial. In a sample of 65 healthy adults, voxelwise regression analyses demonstrated positively-predicted ventral and negatively-predicted dorsal networks associated with the total amygdala, consistent with previous animal and human studies. Investigation of individual amygdala subdivisions revealed distinct differences in connectivity patterns within the amygdala and throughout the brain. Spontaneous activity in the laterobasal subdivision predicted activity in temporal and frontal regions, while activity in the centromedial nuclei predicted activity primarily in striatum. Activity in the superficial subdivision positively predicted activity throughout the limbic lobe. These findings suggest that resting state fMRI can be used to investigate human amygdala networks at a greater level of detail than previously appreciated, allowing for the further advancement of translational models.

The central role of the amygdala in processing emotions and mediating fear responses is well established (LeDoux, 2000). Tucked away in the medial temporal lobe and comparatively small in size, the human amygdala is not easily studied in vivo. Further, the amygdala is not a single structure, but a complex of structurally and functionally heterogeneous nuclei which have been examined extensively in rodents and non-human primates, but not in humans. In recent years, advances have also been made in the study of the amygdaloid complex in humans. For example, using cytoarchitectonic mapping methods similar to those used in animal studies, Amunts et al. (2005) delineated probabilistic maps of amygdala subregions. Neuroimaging studies have

Corresponding Author: Amy Krain Roy, Ph.D., NYU Child Study Center, 215 Lexington Avenue, 13th Floor, New York, N.Y. 10016, Phone: (212) 263-2790, Fax: (212) 263-3691, amy.roy@nyumc.org.

also demonstrated structural (Sheline et al., 1998) as well as functional (Morris et al., 2001; Ball et al., 2007; Kim et al., 2003; Whalen et al., 2004) distinctions in the human amygdala that parallel those observed in animals. Translational models implicating specific amygdala nuclei in processes such as fear learning and extinction are beginning to inform our understanding of anxiety and related psychopathology in humans, making more detailed evaluations of the amygdala and its circuits even more essential (Davis, 2006; Akirav and Maroun, 2007).

Considering the amygdala as a single unit, as is common in most human neuroimaging studies, potentially overlooks the independent functions and patterns of connectivity of individual subdivisions (laterobasal, centromedial, and superficial), and their component nuclei, that have been discerned in animals (Pitkanen, 2000; Russchen et al., 1985; Davis, 2006). The laterobasal group of nuclei includes the lateral, basolateral, basomedial, and basoventral nuclei. These nuclei facilitate associative learning processes such as fear conditioning through afferents from cortical and subcortical regions, including thalamus, hippocampus, and prefrontal cortex (LeDoux, 2003; Phelps and LeDoux, 2005). The centromedial group, composed of the central and medial nuclei, plays a significant role in generating behavioral responses through projections to the brainstem, as well as cortical and striatal regions such as the caudate (Davis, 1997; LeDoux, 2003). The superficial subdivision of the amygdala lies adjacent to the laterobasal group and includes the cortical nuclei involved in olfactory (Heimer and Van Hoesen, 2006; Price, 2003) and affective processes (Gonzalez-Lima and Scheich, 1986).

Task-based fMRI studies have begun to identify distinct patterns of activation in subregions of the amygdala, primarily making distinctions between dorsal and ventral areas (Morris et al., 2001; Kim et al., 2003; Whalen et al., 2004). A recent paper by Ball et al. (2007) examined specific functional differences among the laterobasal, centromedial, and superficial amygdala subdivisions. Using probabilistic anatomic maps of these subdivisions (Amunts et al., 2005), the authors showed positive signal changes in laterobasal amygdala and negative signal changes in superficial and centromedial subdivisions in response to auditory stimuli. These data are the first to demonstrate functional distinctions of amygdala subdivisions (laterobasal, centromedial, and superficial) in the human brain, supporting the utility of using such probabilistic anatomic maps to guide interpretations of functional neuroimaging data.

Studies of the functional connectivity of the human amygdala have typically examined it as a single unit, finding results generally consistent with known anatomic connections in non-human primates (Amaral and Price, 1984; Amaral, 1986). For example, Stein et al. (2007) demonstrated significant associations between activation in the amygdala and parahippocampal gyrus, anterior cingulate cortex, orbitofrontal cortex, posterior cingulate, and insula. The most replicated of these associations is the correlation between activity in prefrontal regions (e.g., anterior cingulate cortex, ventral prefrontal cortex, orbitofrontal cortex) and the amygdala, which is believed to provide the basis for emotion regulation processes (Hariri et al., 2003; Ochsner et al., 2004; Zald and Pardo, 1997).

The aim of the current investigation is to build upon the novel work of Ball et al. (2007) by examining unique connectivity patterns of the laterobasal, centromedial, and superficial subdivisions of the amygdala using resting state functional MRI. Resting state functional connectivity is a highly effective and efficient method for mapping complex neural circuits that is thought to reflect the underlying neuroanatomy (Andrews-Hanna et al., 2007; Greicius et al., 2008; Vincent et al., 2007; Hagmann et al., 2008). Prior work by our lab demonstrates the power of this method to detect differential patterns of functional connectivity for subregions of the anterior cingulate cortex (ACC) (Margulies et al., 2007) and striatum (Di Martino et al., 2008) that are consistent with meta-analyses of human functional data (Koski & Paus, 2000; Postuma & Dagher, 2006) and anatomic data from non-human primates and rodents

(Alexander, DeLong, & Strick, 1986; Devinsky, Morrell, & Vogt, 1995). The current study uses similar methods to examine whether amygdala-based networks identified in animal models can be detected in humans using resting- state fMRI. By exploring intrinsic spontaneous low-frequency correlations in BOLD signal, we are able to map patterns of connectivity in both hemispheres without relying on task-related activations that are often variable (Hariri et al., 2000; Lange et al., 2003), and likely differ from spontaneous amygdala activity (Zald et al., 1998).

Materials and Methods

Participants

Sixty-five right-handed (as assessed by the Edinburgh Handedness Inventory; Oldfield, 1971) native English-speaking participants with no history of psychiatric or neurological illness (confirmed by psychiatric clinical assessment) were enrolled (33 males; mean age: 29.3 ± 7.9 years). The study was approved by the NYU School of Medicine and New York University institutional review boards. Signed informed consent was obtained prior to participation.

Data Acquisition and Image Preprocessing

Resting state data were acquired on a Siemens Allegra 3.0 Tesla scanner. During the scan, participants were instructed to rest with their eyes open while the word “Relax” was centrally projected in white, against a black background. The reliability of functional connectivity analyses has been demonstrated across resting state conditions (i.e., eyes open, eyes closed) (Fox et al., 2005; Fransson, 2005). There was no evidence that participants had fallen asleep during the scan, although this was not directly measured. We collected 197 contiguous EPI functional volumes (TR = 2000 ms; TE = 25 ms; flip angle = 90, 39 slices, matrix = 64x64; FOV = 192 mm; acquisition voxel size = 3x3x3mm). For spatial normalization and localization, a T1-weighted anatomical image (MPRAGE, TR = 2500ms; TE = 4.35ms; TI = 900ms; flip angle = 8; 176 slices, FOV = 256 mm) was also obtained. Subsets of these data have been used in previous studies of functional connectivity (Castellanos et al., 2008; Di Martino et al., 2008; Kelly et al., 2008; Kelly et al., in press; Margulies et al., 2007; Uddin et al., 2007; Uddin et al., 2008). Image preprocessing was carried out using AFNI (http://afni.nimh.nih.gov/afni/) and FSL (www.fmrib.ox.ac.uk). Preprocessing using AFNI consisted of (1) slice time correction (first slice as reference, interleaved acquisitions, Fourier interpolation), (2) 3D motion correction, and (3) despiking (removal of extreme timeseries outliers). Preprocessing using FSL consisted of (4) spatial smoothing (FWHM = 6mm), (5) mean-based intensity normalization of all volumes by the same factor, (6) temporal highpass filtering (Gaussian-weighted least-squares straight line fitting, sigma = 100.0s), and (7) correction for time series autocorrelation (pre-whitening) using FILM (FMRIB’s Improved Linear Model), which calculates voxelwise pre-whitening matrices (Woolrich, Ripley, Brady, & Smith, 2001). Temporal lowpass filtering (Gaussian filter, HWHM = 2.8s) was also performed using FSL in order to isolate the low-frequency BOLD fluctuations of interest. Previous studies have found this range to have the greatest power in BOLD signal (Biswal, Yetkin, Haughton, & Hyde, 1995; Fransson, 2006), the strongest correlations between regions (Achard, Salvador, Whitcher, Suckling, & Bullmore, 2006), and to relate most closely to task-based activations (Fox, Snyder, Vincent, & Raichle, 2007; Fransson, 2006; Toro, Fox, & Paus, 2008) and underlying structural connectivity (Greicius, Supekar, Menon, & Dougherty, 2008; Hagmann et al., 2008; Vincent et al., 2007). Functional data were then transformed into MNI space using a 12 degree of freedom linear affine transformation implemented in FLIRT (voxel size = 2 × 2 × 2 mm), to enable time series extraction using standard anatomical masks.

Functional Connectivity: Time Series Extraction

Our goal was to examine differential patterns of connectivity among the laterobasal, centromedial, and superficial subdivisions of the amygdala using the same regional definitions as Ball et al. (2007). Regions of interest (ROIs) were determined using stereotaxic, probabilistic maps of cytoarchitectonic boundaries developed by Amunts et al. (2005) and implemented in FSL's Juelich histological atlas (Figure 1). The laterobasal (LB) subdivision (Left: 1840 mm^3, Right: 1920 mm^3) includes the lateral, basolateral, basomedial, and paralaminar nuclei. The centromedial (CM) subdivision (Left: 176 mm^3, Right: 224 mm^3) consists of the central and medial nuclei. The superficial (SF) subdivision (Left: 952 mm^3, Right: 760 mm^3) includes the anterior amygdaloid area, the amygdalopyriform transition area, the amygdaloid-hippocampal area and the ventral and posterior cortical nuclei. We created our regions of interest in standard space, including only voxels with a probability of at least 50% of belonging to each subdivision (LB, CM, SF). Each voxel was assigned to only one subdivision. In cases of overlap, such voxels were assigned to the region for which they had the highest probability of inclusion. To minimize effects due to interindividual anatomic variability, each voxel's time series was weighted by the probability of inclusion in a given amygdala subdivision, based on the interindividual variability of the ten subjects used to construct the original anatomic atlas (Amunts et al., 2005). In other words, those voxels most reliably located in a given region made the greatest contribution to its signal. In each subject, mean time series were then extracted by averaging across all voxels' probability-weighted time series within each subdivision. Additional analyses were conducting using amygdala ROIs with more and less conservative thresholds. First, we used a more liberal 25% threshold with results similar to those of the original 50% analyses. Second, to increase the specificity of our amygdala subdivisions, we created ROIs that represented the 'core' components of each subdivision. We took each of the 50% probability masks and rank ordered the probability values of each voxel and then restricted each ROI to only include voxels with the top 20 probability values. Using these 'core' ROIs, we generated voxelwise functional connectivity maps using the same methods used for the primary analysis using 50% probability ROIs. Cross-correlations of the resulting maps were found to be highly significant (all comparisons $r > 0.94$; $p < 10^{-4}$) with the maps generated with 50% probability ROIs (see Supplementary Figure).

Probabilistic maps were not available for the total amygdala; therefore, binary composite masks (Left: 2968 mm^3, Right: 2904 mm^3) were created by combining the individual subdivision masks, each thresholded at a probability of 50% for the right and left amygdala separately. Mean time series were then calculated by averaging across all voxels within each mask.

Functional Connectivity: Statistical Analysis

As outlined in Margulies et al. (2007), multiple regression analyses were performed for each subject using FSL's FEAT. For each hemisphere, a regression model (GLM) was created which included each of the three amygdala subdivision time series predictors and nine nuisance covariates (time series predictors for global signal, white matter, cerebrospinal fluid, and six motion parameters). The global signal is thought to reflect a combination of physiological processes (i.e., cardiac and respiratory fluctuations), and therefore, was included in the GLM to control for such factors. Within these regression models, the LB, CM, and SF time series from each hemisphere were orthogonalized (using the Gram-Schmidt process) with respect to each other, and with respect to the nuisance covariates, to ensure that the time series for each ROI reflected its unique variance. This analysis produced individual subject-level maps of all positively-and negatively-predicted voxels for each regressor. To test whether orthogonalization was leading to underestimation of functional connectivity, analyses were repeated with each amygdala subdivision in a separate regression model. Results were highly similar to those found with orthogonalization; therefore, only the orthogonalized results are presented here. To examine the functional connectivity of the amygdala as a whole, separate

regression models were created for each hemisphere that included the total amygdala time series along with the same nine nuisance variables used for the subdivision analyses.

Group-level analyses, controlling for age and gender, were conducted using FLAME, a mixed-effects model implemented in FSL. Cluster-based corrections for multiple comparisons used gaussian random field theory ($Z > 2.3$; cluster significance: $p < 0.05$, corrected) resulting in thresholded z-score maps of correlated voxels associated with each amygdala subdivision and the total amygdala for each hemisphere. Direct comparisons were conducted to verify differences in functional connectivity across amygdala subdivisions: CM vs. SF+LB, LB vs. SF+CM, and SF vs. CM+LB. When we observed that the functional connectivity of right and left amygdala subdivisions differed in that one uniquely predicted the activity of a specific region, we conducted follow-up analyses. These consisted of paired samples t-tests with hemisphere (right vs. left) as the independent variable and parameter estimates for the region of interest as the dependent variable. To directly examine areas of convergence among the laterobasal, centromedial, and superficial amygdala subdivisions, we conducted a conjunction analysis by overlaying the thresholded maps for each subdivision. Only those voxels which survived correction for each subdivision were included, resulting in maps of positive and negative functional connectivity patterns common to all three amygdala subdivisions.

Given the amygdala's limited spatial extent, additional analyses were conducted using decreased spatial smoothing (FWHM = 4.5mm). Although less robust, patterns of connectivity were consistent with those of primary analyses and therefore are not reported here.

Results

Total Amygdala

Spontaneous activity in the amygdala positively predicted spontaneous activity in medial prefrontal regions including medial frontal gyrus (BA 10) and rostral ACC (BA32), as well as a small region of dorsal ACC (BA 24). Other regions positively predicted by amygdala activity included insula, thalamus, and striatum. Conversely, amygdala activity negatively predicted activity in dorsal and posterior regions such as superior frontal gyrus (BA 6/8), bilateral middle frontal gyrus, posterior cingulate cortex (PCC), precuneus (BA 7), and parietal and occipital lobes bilaterally (Tables 1 & 2; Figure 2). Overall, these patterns of functional connectivity were similar for the left and right amygdala and support models of emotion processing that suggest reciprocal ventral and dorsal systems (Phillips et al., 2003).

Amygdala Subdivisions

Laterobasal—Spontaneous activity in LB nuclei predicted bilateral activity primarily in temporal regions including the hippocampus, parahippocampal gyrus, and superior temporal gyrus (Tables 3 & 4; Figure 2). Direct comparisons verified that these positive associations were significantly greater for the LB subdivision than either CM or SF subdivisions (Figure 3) Additionally, spontaneous activity in the right LB nuclei predicted activity in medial prefrontal regions including medial frontal gyrus (BA 11), superior frontal gyrus (BA 10), anterior cingulate cortex (BA 32), and dorsal regions including precentral and postcentral gyri, bilaterally. Direct comparison between hemispheres found that LB functional connectivity with medial prefrontal regions did not differ significantly ($t[64] = =1.24$, $p = .22$) suggesting connectivity at a subthreshold level ($p > .05$) (Figure 4A). Similar analyses found significant hemispheric differences in LB functional connectivity with regions of the precentral gyrus ($t[64] = -3.10$, $p = .003$) suggesting that this association is unique to the right LB. These results support animal studies demonstrating significant connectivity between nuclei in the LB subdivision and prefrontal and temporal regions, facilitating their role in associative learning processes (Schoenbaum et al., 2000).

While regions positively associated with the LB nuclei were primarily in temporal and frontal regions, negatively associated loci were located in dorsal and posterior regions such as dorsal ACC, extending from BA 24 to BA 32, middle frontal gyrus (BA 6/9), PCC, precuneus, bilateral parietal lobe, and cerebellum (Figure 2). Thalamus, caudate, and superficial amygdala were also negatively predicted by spontaneous LB activity. Negative associations with most regions were greater for the LB nuclei than for the other two subdivisions (Figure 3). Overall, the connectivity patterns of the LB subdivision, specifically positive predictions of spontaneous activity in rostral ACC and medial prefrontal cortex (PFC) and negative predictions of activity in dorsal ACC and middle frontal gyrus, are consistent with emotion regulation circuits previously delineated in task-based studies (Hariri et al., 2000;Hariri et al., 2003;Ochsner et al., 2004).

Centromedial—Spontaneous activity in the CM subdivision positively predicted activity in the striatum, with significant clusters detected bilaterally, extending from the nucleus accumbens into dorsal portions of the caudate and nearby portions of the putamen. Additionally, areas of significant connectivity were detected in the globus pallidus, dorsal ACC, insula, and cerebellum (Tables 5 & 6; Figure 2). Direct comparison with the LB and SF groups found that the CM nuclei showed significantly greater functional connectivity with caudate, putamen, globus pallidus, thalamus, cerebellum, and dorsal ACC (Figure 3). These findings support the role of the CM as an output region of the amygdala, facilitating motor responding, reward processing, and increased attention and cortical readiness (Davis, 1997).

Regions negatively predicted by activity in the left and right CM groups were primarily in posterior regions including precuneus and occipital lobe (Figure 2). Spontaneous activity in the right CM uniquely negatively predicted activity in ventral regions of the right amygdala (including SF and LB nuclei), medial frontal gyrus, and left middle frontal gyrus. This was confirmed by direct comparisons showing significant differences in the functional connectivity of left and right CM with each of these regions (amygdala: $t[64] = 10.44$, $p = .001$; medial frontal gyrus: $t[64] = 3.67$, $p = .001$; middle frontal gyrus: $t[64] = 2.78$, $p = .007$) (Figure 4B). These regions of amygdala and medial frontal gyrus overlapped considerably with regions positively predicted by spontaneous activity in the LB subdivision (Figure 5A). These findings, in addition to the positively predicted activity in regions of the striatum that are negatively predicted by activity in LB nuclei (Figure 5B), may reflect reciprocal response patterns resulting from inhibitory relationships between LB and CM nuclei that have been observed in animals (Collins & Pare, 1999).

Superficial—The SF subdivision demonstrated patterns of functional connectivity that are consistent with traditional models of the “limbic lobe” (Morgane et al., 2005). Left and right SF groups positively predicted spontaneous activity in regions along the cingulate gyrus extending from subgenual cingulate to dorsal ACC (BA 24) (Tables 7 & 8; Figure 2). Positive associations were also found in insula, striatum (caudate, nucleus accumbens), and hippocampus. Direct comparisons with the LB and CM groups found greater functional connectivity between the SF group and these areas, except lateral and posterior temporal regions for the left SF subdivision (Figure 3). The overall pattern of activity significantly predicted in limbic regions suggests that olfactory processes associated with the cortical nuclei of the SF group may continue to play a key affective role in humans, as they do in animals (Price, 2003).

Spontaneous activity in the SF subdivision negatively predicted activity in posterior regions such as the angular gyrus, superior parietal lobe, and cerebellum and frontal regions including the middle frontal gyrus (BA 6, 8, 9). Direct comparisons with the LB and CM subdivisions found negative associations between the right SF and frontal and parietal regions mostly in the contralateral hemisphere. Direct comparisons of the left SF subdivision with the CM and LB

subdivisions only showed significant differences posteriorly, in the cerebellum and bilateral angular gyrus (Figure 3).

Conjunction Analysis—To examine regions of convergence among the amygdala subdivisions, we conducted an overlay analysis of thresholded maps from each subdivision. Only those voxels that reached corrected significance in each of the 3 subdivision analyses were included. As a result, we found significant convergence in insular cortex for positive FC and posterior regions (precuneus, lateral occipital cortex) for negative FC (see Figure 6).

Discussion

By mapping temporally correlated patterns of low frequency spontaneous activity during rest, we detected distinct functional networks associated with three amygdala subdivisions. These results demonstrate the potential of resting state fMRI to make fine-tuned distinctions within amygdala circuits in vivo, and as such, contribute to the growing literature supporting translational models of amygdala function.

Analyses of the amygdala as a single region revealed patterns of functional connectivity largely consistent with animal models (Pitkanen, 2000; Amaral and Price, 1984), and task-based human neuroimaging findings (Stein et al., 2007). Spontaneous activity in the amygdala positively predicted activity in regions implicated in identifying the emotional significance of stimuli and producing affective states; these include ACC, insula, medial PFC, striatum, and thalamus. Conversely, activity in regions involved in cognitive processes and effortful regulation of affect, such as superior frontal gyrus, middle frontal gyrus, PCC, and precuneus, was negatively predicted by amygdala activity.

The functional connectivity of individual amygdala subdivisions showed regions of overlap and regions uniquely related to each subdivision. The insular cortex represented a region of convergence for positive functional connectivity maps while the precuneus and lateral occipital cortex represented regions of convergence for negative functional connectivity maps. The unique patterns of connectivity associated with each amygdala subdivision revealed homologies with animal amygdala-based circuits at a level of resolution greater than previously considered by most human imaging studies. Consistent with its role in associative learning processes such as contextual fear conditioning (LeDoux, 2000; Phelps and LeDoux, 2005), the laterobasal subdivision was positively associated with activity in the superior temporal gyrus, hippocampus, and parahippocampal gyrus. Additionally, this subdivision positively predicted activity in medial PFC and precentral gyrus; this latter association was significantly stronger for the right LB than the left. These connectivity patterns, along with negative associations between spontaneous fluctuations in the LB subdivision and dorsal and posterior regions such as dorsal ACC, middle frontal gyrus, and precuneus, are consistent with data from previous task-based studies demonstrating the involvement of similar circuits in emotion regulation (Hariri et al., 2000; Ochsner et al., 2004; Phelps and LeDoux, 2005; Phillips et al., 2003; Zald, 2003; Blair et al., 2007). Activity of the centromedial nuclei, which mediate response expression and facilitate attention to salient stimuli (Kapp et al., 1994), was significantly correlated with thalamus, insula, dorsal ACC, and cerebellum. Significant positive associations were also found with striatal regions (caudate, putamen, GP) which are similar in function, connectivity, and chemistry (neurotransmitter and peptide distribution) to the centromedial nuclei (Swanson and Petrovich, 1998; Swanson, 2003). The superficial nuclei, which support olfactory information processing and olfaction-related affective processing in rodents (Kemppainen et al., 2002; Pitkanen, 2000), positively predicted activity throughout regions traditionally identified as limbic cortex including the cingulate gyrus extending from subgenual to dorsal regions, insula, and striatum.

The merits of examining individual amygdala subdivisions are further highlighted by findings that some regions showed opposing patterns of connectivity with different amygdala subdivisions. This was particularly evident in patterns of connectivity involving the centromedial and laterobasal subdivisions. Positively-predicted laterobasal and negatively-predicted centromedial networks converged in regions of medial PFC and temporal lobe while negatively-predicted laterobasal and positively-predicted centromedial networks converged in the striatum. Even within the amygdala, resting state activity of the right centromedial subdivision negatively predicted activity in the laterobasal subdivision. This is consistent with reports of reciprocal oscillations in the firing probabilities of lateral and centromedial nuclei observed in animals (Collins and Pare, 1999) and opposing BOLD activation patterns in these same regions observed in humans (Ball et al., 2007).

While our results were generally consistent with the extant literature, there was evidence of functional connectivity patterns that do not have clear anatomic bases. These findings highlight the fact that our methods measure correlated spontaneous activity, which may reflect indirect as well as direct anatomic connections (Greicius, Supekar, Menon, & Dougherty, 2008; Hagmann et al., 2008; Vincent et al., 2007). Further, the mechanisms underlying negative relationships between brain regions detected with resting-state fMRI remain unknown (Fox et al., 2005; Fransson, 2005). These findings also suggest that the functional connectivity of human amygdala subdivisions may differ somewhat from that of non-human primates and rodents. Future studies applying these resting state FC methods to translational research could provide the means for more effective comparisons of amygdala circuitry across species.

We observed a high degree of concordance in the functional connectivity of the left and right amygdala. These findings are consistent with previous investigations of resting state connectivity across the brain (Lowe et al., 1998; Biswal et al., 1995) and of the amygdala (Zald et al., 1998). However, lateralized patterns of correlated spontaneous activity were also observed, particularly for the right centromedial subdivision, which demonstrated a unique negative association with activity in the superficial/laterobasal amygdala, medial frontal gyrus, and left middle frontal gyrus. These results may reflect structural differences, as the right centromedial subdivision was 25% larger than the left, allowing for greater power to detect negative associations. Ball et al. (2007) found a similar lateralization of responses in the centromedial subdivision (positive responses on the right and negative responses on the left) that was not observed in the LB or SF subdivisions. The concordance of these findings suggests that lateralization in regulation of amygdala activity may be observed at a more detailed level. For example, there is some evidence that the right amygdala demonstrates more rapid habituation to fearful faces than the left amygdala (Phillips et al., 2001; Wright et al., 2002). This may result from greater negative intrinsic connectivity between the right CM subdivision and regions involved in fear learning (laterobasal nuclei) (LeDoux, 2003; Phelps and LeDoux, 2005) as well as the regulation of emotion (medial frontal gyrus) (Hariri et al., 2003; Irwin et al., 2004; Berretta, 2003). Clearly, these ideas are speculative and additional studies of the connectivity of the amygdala subdivisions at rest, as well as during task, are needed to further investigate these questions of laterality.

The current study delineated patterns of connectivity that have been shown to be altered in clinical populations using task-based methods (Heinz et al., 2005; McClure et al., 2007; Pezawas et al., 2005; Quirk and Gehlert, 2003). This suggests that resting state fMRI can be used to efficiently probe intrinsic differences in these critical circuits without the potential confounds of group differences in task performance. Further, by observing significant differences in the connectivity of amygdala subdivisions implicated in fear learning and extinction, we demonstrate the utility of these methods for testing translational models of fear and anxiety. For example, pharmacological treatments that affect the basolateral amygdala in animals are effective at facilitating extinction in patients with anxiety disorders (Hofmann,

2007; McNally, 2007; Davis et al., 2006). Our methods may provide an opportunity to further examine the impact of these agents on amygdala circuits in humans.

The present study has several limitations. First, our results only apply to resting state data and may not reflect connectivity during task performance. However, the convergence of these findings with those from animal studies suggests that intrinsic activity likely indexes functionally relevant circuits. Furthermore, recent studies using diffusion tensor imaging (DTI; Greicius et al., 2008) and task-based meta-analyses (Toro et al., 2008) suggest that functional connectivity reflects structural connectivity and that networks identified in the resting-state mimic those identifiable across a wide array of task paradigms, respectively. Second, the amygdala is susceptible to EPI image distortions, normalization errors, and draining vein effects which may lead to spatial localization errors (Merboldt, Fransson, Bruhn, & Frahm, 2001). As such, connectivity patterns reported for a given amygdala subdivision could, to some extent reflect surrounding structures. This problem would likely be greatest for the CM as it is the smallest of the three subdivisions. To minimize these effects on localization of amygdala subdivisions, we used probabilistic maps of amygdala ROIs with a 50% threshold (only voxels with a probability of 50% or higher of belonging to that region were included) and probability-weighted each voxel's contribution to the time series. We also conducted more conservative analyses to further reduce the effect of spatial errors. Using only the twenty voxels for each subdivision that had the highest probability of membership, we found highly similar results (cross-correlations between thresholded maps $p < 10^{-4}$). While these analyses do not eliminate the likely impact of distortion and localization errors, they provide initial evidence that independent functional connectivity patterns can be identified within the amygdala. Future fMRI studies using coronal sections, smaller voxel sizes, and EPI distortion correction will help to further confirm the localization of amygdala subdivisions and the current findings. Third, while our results suggest functional connectivity between amygdala subdivisions and anterior regions of the cerebellum, we were not able to extend analyses to more inferior cerebellar structures due to our imaging parameters, which limited coverage in these regions. Fourth, we selected the laterobasal, centromedial, and superficial subdivisions based upon the most recent structural delineation of amygdala subdivisions in humans (Amunts et al., 2005), which is still less detailed than animal models.

In summary, resting state fMRI was used to interrogate human amygdala-based circuits at a greater level of detail than previously examined. The convergence of these findings with animal models supports the validity of this approach for the translational investigation of amygdala networks and their role in psychopathology and development.

Supplementary Material

Refer to Web version on PubMed Central for supplementary material.

Acknowledgments

The authors wish to thank David Stark and Katie Hiler for their assistance with supplementary materials and are grateful to those individuals who volunteered their time to participate in this study. This work was supported in part by NIMH (K23 MH074821).

Reference List

Achard S, Salvador R, Whitcher B, Suckling J, Bullmore E. A resilient, low-frequency, small-world human brain functional network with highly connected association cortical hubs. J Neurosci 2006;26:63–72. [PubMed: 16399673]

Akirav I, Maroun M. The role of the medial prefrontal cortex-amygdala circuit in stress effects on the extinction of fear. Neural Plast 2007:30873. [PubMed: 17502909]

Alexander GE, DeLong MR, Strick PL. Parallel organization of functionally segregated circuits linking basal ganglia and cortex. Annu Rev Neurosci 1986;9:357–381. [PubMed: 3085570]

Amaral DG. Amygdalohippocampal and amygdalocortical projections in the primate brain. Adv Exp Med Biol 1986;203:3–17. [PubMed: 3788708]

Amaral DG, Price JL. Amygdalo-cortical projections in the monkey (Macaca fascicularis). J Comp Neurol 1984;230:465–496. [PubMed: 6520247]

Amunts K, Kedo O, Kindler M, Pieperhoff P, Mohlberg H, Shah NJ, Habel U, Schneider F, Zilles K. Cytoarchitectonic mapping of the human amygdala, hippocampal region and entorhinal cortex: intersubject variability and probability maps. Anat Embryol (Berl) 2005;210:343–352. [PubMed: 16208455]

Andrews-Hanna JR, Snyder AZ, Vincent JL, Lustig C, Head D, Raichle ME, Buckner RL. Disruption of large-scale brain systems in advanced aging. Neuron 2007;56:924–935. [PubMed: 18054866]

Ball T, Rahm B, Eickhoff SB, Schulze-Bonhage A, Speck O, Mutschler I. Response properties of human amygdala subregions: evidence based on functional MRI combined with probabilistic anatomical maps. PLoS ONE 2007;2:e307. [PubMed: 17375193]

Berretta S. Local release of GABAergic inhibition in the medial prefrontal cortex induces immediate-early genes in selective neuronal subpopulations in the amygdala. Annals of the New York Academy of Sciences 2003;985:505–507.

Biswal BB, Yetkin FZ, Haughton VM, Hyde JS. Functional connectivity in the motor cortex of resting human brain using echoplanar MRI. Magn Reson Med 1995;34:537–541. [PubMed: 8524021]

Blair KS, Smith BW, Mitchell DG, Morton J, Vythilingam M, Pessoa L, Fridberg D, Zametkin A, Sturman D, Nelson EE, Drevets WC, Pine DS, Martin A, Blair RJ. Modulation of emotion by cognition and cognition by emotion. Neuroimage 2007;35:430–440. [PubMed: 17239620]

Castellanos FX, Margulies DS, Kelly C, Uddin LQ, Ghaffari M, Kirsch A, Shaw D, Shehzad Z, Di Martino A, Biswal B, Sonuga-Barke EJ, Rotrosen J, Adler LA, Milham MP. Cingulate-precuneus interactions: a new locus of dysfunction in adult attention-deficit/hyperactivity disorder. Biol Psychiatry 2008;63:332–337. [PubMed: 17888409]

Collins DR, Pare D. Reciprocal changes in the firing probability of lateral and central medial amygdala neurons. J Neurosci 1999;19:836–844. [PubMed: 9880603]

Davis M. Neurobiology of fear responses: the role of the amygdala. J Neuropsychiatry Clin Neurosci 1997;9:382–402. [PubMed: 9276841]

Davis M. Neural systems involved in fear and anxiety measured with fear-potentiated startle. Am Psychol 2006;61:741–756. [PubMed: 17115806]

Davis M, Ressler K, Rothbaum BO, Richardson R. Effects of D-cycloserine on extinction: translation from preclinical to clinical work. Biol Psychiatry 2006;60:369–375. [PubMed: 16919524]

Devinsky O, Morrell MJ, Vogt BA. Contributions of anterior cingulate cortex to behaviour. Brain 1995;118 (Pt 1):279–306. [PubMed: 7895011]

Di Martino A, Scheres A, Margulies DS, Kelly AMC, Uddin LQ, Shehzad Z, Biswal B, Walters JR, Castellanos FX, Milham MP. Functional connectivity of the human striatum: a resting state fMRI study. Cerebral Cortex. in press

Fox MD, Snyder AZ, Vincent JL, Raichle ME. Intrinsic fluctuations within cortical systems account for intertrial variability in human behavior. Neuron 2007;56:171–184. [PubMed: 17920023]

Fox MD, Snyder AZ, Vincent JL, Corbetta M, Van Essen DC, Raichle ME. The human brain is intrinsically organized into dynamic, anticorrelated functional networks. Proc Natl Acad Sci U S A 2005;102:9673–9678. [PubMed: 15976020]

Fransson P. Spontaneous low-frequency BOLD signal fluctuations: An fMRI investigation of the resting-state default mode of brain function hypothesis. Human Brain Mapping 2005;26:15–29. [PubMed: 15852468]

Fransson P. How default is the default mode of brain function? Further evidence from intrinsic BOLD signal fluctuations. Neuropsychologia 2006;44:2836–2845. [PubMed: 16879844]

Gonzalez-Lima F, Scheich H. Classical conditioning of tone-signaled bradycardia modifies 2-deoxyglucose uptake patterns in cortex, thalamus, habenula, caudate-putamen and hippocampal formation. Brain Res 1986;363:239–256. [PubMed: 3942896]

Greicius MD, Supekar K, Menon V, Dougherty RF. Resting-state functional connectivity reflects structural connectivity in the default mode network. Cereb Cortex. 2008

Hagmann P, Cammoun L, Gigandet X, Meuli R, Honey CJ, Wedeen VJ, et al. Mapping the structural core of human cerebral cortex. PLoS Biol 2008;6:e159. [PubMed: 18597554]

Hariri AR, Bookheimer SY, Mazziotta JC. Modulating emotional responses: effects of a neocortical network on the limbic system. Neuroreport 2000;11:43–48. [PubMed: 10683827]

Hariri AR, Mattay VS, Tessitore A, Fera F, Weinberger DR. Neocortical modulation of the amygdala response to fearful stimuli. Biol Psychiatry 2003;53:494–501. [PubMed: 12644354]

Heimer L, Van Hoesen GW. The limbic lobe and its output channels: implications for emotional functions and adaptive behavior. Neurosci Biobehav Rev 2006;30:126–147. [PubMed: 16183121]

Heinz A, Braus DF, Smolka MN, Wrase J, Puls I, Hermann D, Klein S, Grusser SM, Flor H, Schumann G, Mann K, Buchel C. Amygdala-prefrontal coupling depends on a genetic variation of the serotonin transporter. Nat Neurosci 2005;8:20–21. [PubMed: 15592465]

Hofmann SG. Enhancing exposure-based therapy from a translational research perspective. Behav Res Ther 2007;45:1987–2001. [PubMed: 17659253]

Irwin W, Anderle MJ, Abercrombie HC, Schaefer SM, Kalin NH, Davidson RJ. Amygdalar interhemispheric functional connectivity differs between the non-depressed and depressed human brain. Neuroimage 2004;21:674–686. [PubMed: 14980569]

Kapp BS, Supple WF Jr, Whalen PJ. Effects of electrical stimulation of the amygdaloid central nucleus on neocortical arousal in the rabbit. Behav Neurosci 1994;108:81–93. [PubMed: 8192853]

Kelly AMC, Di Martino A, Uddin LQ, Shehzad Z, Gee DG, Reiss PT, Margulies DM, Castellanos FX, Milham MP. Development of anterior cingulate functional connectivity from late childhood to early adulthood. Cerebral Cortex. in press

Kelly AMC, Uddin LQ, Biswal BB, Castellanos FX, Milham MP. Competition between functional brain networks mediates behavioral variability. Neuroimage 2008;39:527–537. [PubMed: 17919929]

Kemppainen S, Jolkkonen E, Pitkanen A. Projections from the posterior cortical nucleus of the amygdala to the hippocampal formation and parahippocampal region in rat. Hippocampus 2002;12:735–755. [PubMed: 12542226]

Kim H, Somerville LH, Johnstone T, Alexander AL, Whalen PJ. Inverse amygdala and medial prefrontal cortex responses to surprised faces. Neuroreport 2003;14:2317–2322. [PubMed: 14663183]

Koski L, Paus T. Functional connectivity of the anterior cingulate cortex within the human frontal lobe: a brain-mapping meta-analysis. Exp Brain Res 2000;133:55–65. [PubMed: 10933210]

Lange K, Williams LM, Young AW, Bullmore ET, Brammer MJ, Williams SC, Gray JA, Phillips ML. Task instructions modulate neural responses to fearful facial expressions. Biol Psychiatry 2003;53:226–232. [PubMed: 12559655]

LeDoux J. The emotional brain, fear, and the amygdala. Cell Mol Neurobiol 2003;23:727–738. [PubMed: 14514027]

LeDoux J. The amygdala. Curr Biol 2007;17:R868–R874. [PubMed: 17956742]

LeDoux JE. Emotion circuits in the brain. Annu Rev Neurosci 2000;23:155–184. [PubMed: 10845062]

Lowe MJ, Mock BJ, Sorenson JA. Functional connectivity in single and multislice echoplanar imaging using resting-state fluctuations. Neuroimage 1998;7:119–132. [PubMed: 9558644]

Margulies DS, Kelly AM, Uddin LQ, Biswal BB, Castellanos FX, Milham MP. Mapping the functional connectivity of anterior cingulate cortex. Neuroimage 2007;37:579–588. [PubMed: 17604651]

McClure EB, Monk CS, Nelson EE, Parrish JM, Adler A, Blair RJR, Fromm S, Charney DS, Leibenluft E, Ernst M, Pine DS. Abnormal attention modulation of fear circuit function in pediatric generalized anxiety disorder. Arch Gen Psychiatry 2007;64:97–106. [PubMed: 17199059]

McNally RJ. Mechanisms of exposure therapy: how neuroscience can improve psychological treatments for anxiety disorders. Clin Psychol Rev 2007;27:750–759. [PubMed: 17292521]

Merboldt KD, Fransson P, Bruhn H, Frahm J. Functional MRI of the human amygdala? Neuroimage 2001;14:253–257. [PubMed: 11467900]

Morgane PJ, Galler JR, Mokler DJ. A review of systems and networks of the limbic forebrain/limbic midbrain. Prog Neurobiol 2005;75:143–160. [PubMed: 15784304]

Morris JS, Buchel C, Dolan RJ. Parallel neural responses in amygdala subregions and sensory cortex during implicit fear conditioning. Neuroimage 2001;13:1044–1052. [PubMed: 11352610]

Ochsner KN, Ray RD, Cooper JC, Robertson ER, Chopra S, Gabrieli JD, Gross JJ. For better or for worse: neural systems supporting the cognitive down- and up-regulation of negative emotion. Neuroimage 2004;23:483–499. [PubMed: 15488398]

Oldfield RC. The assessment of handedness: The Edinburgh Inventory. Neuropsychologia 1971;9:97–113. [PubMed: 5146491]

Pezawas L, Meyer-Lindenberg A, Drabant EM, Verchinski BA, Munoz KE, Kolachana BS, Egan MF, Mattay VS, Hariri AR, Weinberger DR. 5-HTTLPR polymorphism impacts human cingulate-amygdala interactions: a genetic susceptibility mechanism for depression. Nat Neurosci 2005;8:828–834. [PubMed: 15880108]

Phelps EA, LeDoux JE. Contributions of the amygdala to emotion processing: from animal models to human behavior. Neuron 2005;48:175–187. [PubMed: 16242399]

Phillips ML, Drevets WC, Rauch SL, Lane R. Neurobiology of emotion perception I: The neural basis of normal emotion perception. Biol Psychiatry 2003;54:504–514. [PubMed: 12946879]

Phillips ML, Medford N, Young AW, Williams L, Williams SC, Bullmore ET, Gray JA, Brammer MJ. Time courses of left and right amygdalar responses to fearful facial expressions. Hum Brain Mapp 2001;12:193–202. [PubMed: 11241871]

Pitkanen, A. Connectivity of the rat amygdaloid complex. In: Aggleton, JP., editor. The Amygdala: A Functional Analysis. Oxford University Press; Oxford: 2000. p. 31-115.

Postuma RB, Dagher A. Basal ganglia functional connectivity based on a meta-analysis of 126 positron emission tomography and functional magnetic resonance imaging publications. Cereb Cortex 2006;16:1508–1521. [PubMed: 16373457]

Price JL. Comparative aspects of amygdala connectivity. Ann N Y Acad Sci 2003;985:50–58. [PubMed: 12724147]

Quirk GJ, Gehlert DR. Inhibition of the amygdala: key to pathological states? Ann N Y Acad Sci 2003;985:263–272. [PubMed: 12724164]

Russchen FT, Bakst I, Amaral DG, Price JL. The amygdalostriatal projections in the monkey. An anterograde tracing study. Brain Res 1985;329:241–257. [PubMed: 3978445]

Schoenbaum G, Chiba AA, Gallagher M. Changes in functional connectivity in orbitofrontal cortex and basolateral amygdala during learning and reversal training. J Neurosci 2000;20:5179–5189. [PubMed: 10864975]

Sheline YI, Gado MH, Price JL. Amygdala core nuclei volumes are decreased in recurrent major depression. Neuroreport 1998;9:2023–2028. [PubMed: 9674587]

Stein JL, Wiedholz LM, Bassett DS, Weinberger DR, Zink CF, Mattay VS, Meyer-Lindenberg A. A validated network of effective amygdala connectivity. Neuroimage 2007;36:736–745. [PubMed: 17475514]

Swanson LW, Petrovich GD. What is the amygdala? Trends Neurosci 1998;21:323–331. [PubMed: 9720596]

Swanson LW. The amygdala and its place in the cerebral hemisphere. Ann N Y Acad Sci 2003;985:174–184. [PubMed: 12724158]

Toro R, Fox PT, Paus T. Functional coactivation map of the human brain. Cereb Cortex. 2008

Uddin LQ, Clare Kelly AM, Biswal BB, Xavier CF, Milham MP. Functional connectivity of default mode network components: Correlation, anticorrelation, and causality. Hum Brain Mapp. 2008

Uddin LQ, Kelly AM, Biswal BB, Margulies DS, Shehzad Z, Shaw D, Ghaffari M, Rotrosen J, Adler LA, Castellanos FX, Milham MP. Network homogeneity reveals decreased integrity of default-mode network in ADHD. J Neurosci Methods 2007;169:249– 254. [PubMed: 18190970]

Vincent JL, Patel GH, Fox MD, Snyder AZ, Baker JT, Van Essen DC, Zempel JM, Snyder LH, Corbetta M, Raichle ME. Intrinsic functional architecture in the anaesthetized monkey brain. Nature 2007;447:83– 86. [PubMed: 17476267]

Whalen PJ, Kagan J, Cook RG, Davis FC, Kim H, Polis S, McLaren DG, Somerville LH, McLean AA, Maxwell JS, Johnstone T. Human amygdala responsivity to masked fearful eye whites. Science 2004;306:2061. [PubMed: 15604401]

Woolrich MW, Ripley BD, Brady M, Smith SM. Temporal autocorrelation in univariate linear modeling of FMRI data. Neuroimage 2001;14:1370–1386. [PubMed: 11707093]

Wright CI, Martis B, Shin LM, Fischer H, Rauch SL. Enhanced amygdala responses to emotional versus neutral schematic facial expressions. Neuroreport 2002;13:785–790. [PubMed: 11997687]

Zald DH, Donndelinger MJ, Pardo JV. Elucidating dynamic brain interactions with across-subjects correlational analyses of positron emission tomographic data: the functional connectivity of the amygdala and orbitofrontal cortex during olfactory tasks. J Cereb Blood Flow Metab 1998;18:896–905. [PubMed: 9701351]

Zald DH, Pardo JV. Emotion, olfaction, and the human amygdala: amygdala activation during aversive olfactory stimulation. Proc Natl Acad Sci U S A 1997;94:4119–4124. [PubMed: 9108115]

Zald DH. The human amygdala and the emotional evaluation of sensory stimuli. Brain Res Brain Res Rev 2003;41:88–123. [PubMed: 12505650]

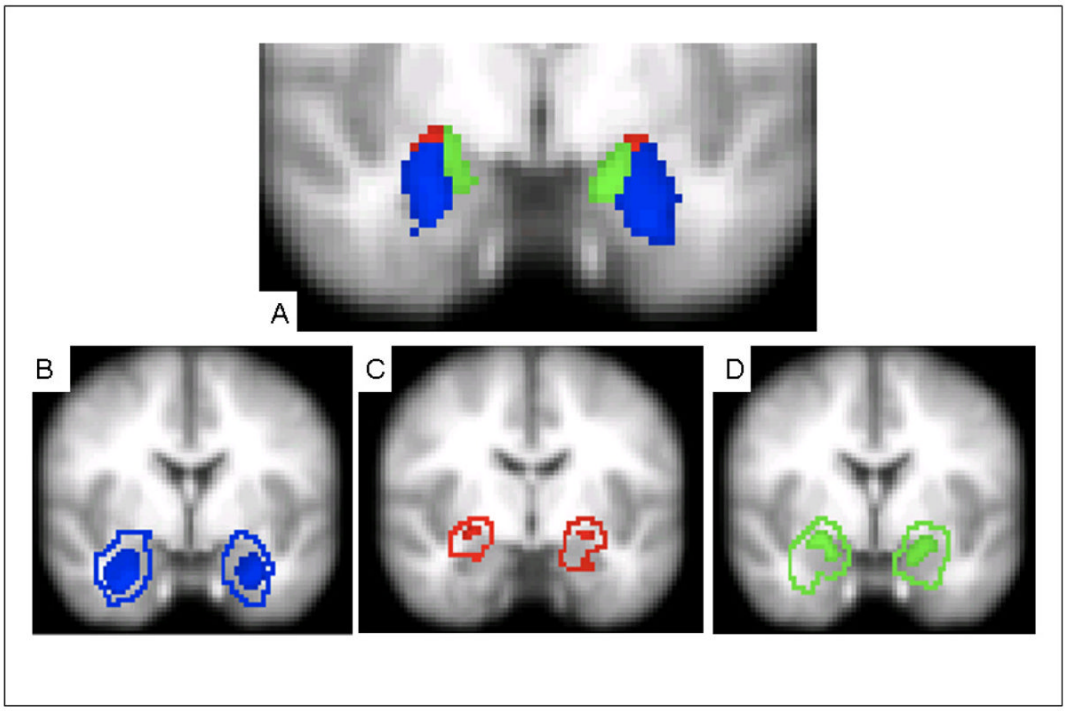

Figure 1.
Location of 50% probabilistic masks of centromedial (CM), laterobasal (LB), and superficial (SF) amygdala projected on a mean EPI image using radiological convention. A) CM, LB, and SF masks (y = −6; Montreal Neurological Institute [MNI] standard space). B) 50% probabilistic mask of LB (solid) with extent of total LB according to the Juelich histological atlas as implemented in FSL (outline) (y = −2); C) 50% probabilistic mask of CM (solid) with extent of total CM according to the Juelich histological atlas as implemented in FSL (outline) (y = −8); D) 50% probabilistic mask of SF (solid) with extent of total SF according to the Juelich histological atlas as implemented in FSL (outline) (y = −2). Subdivision boundaries obtained from the Juelich histological atlas are based on probabilistic maps created by Amunts et al. (2005).

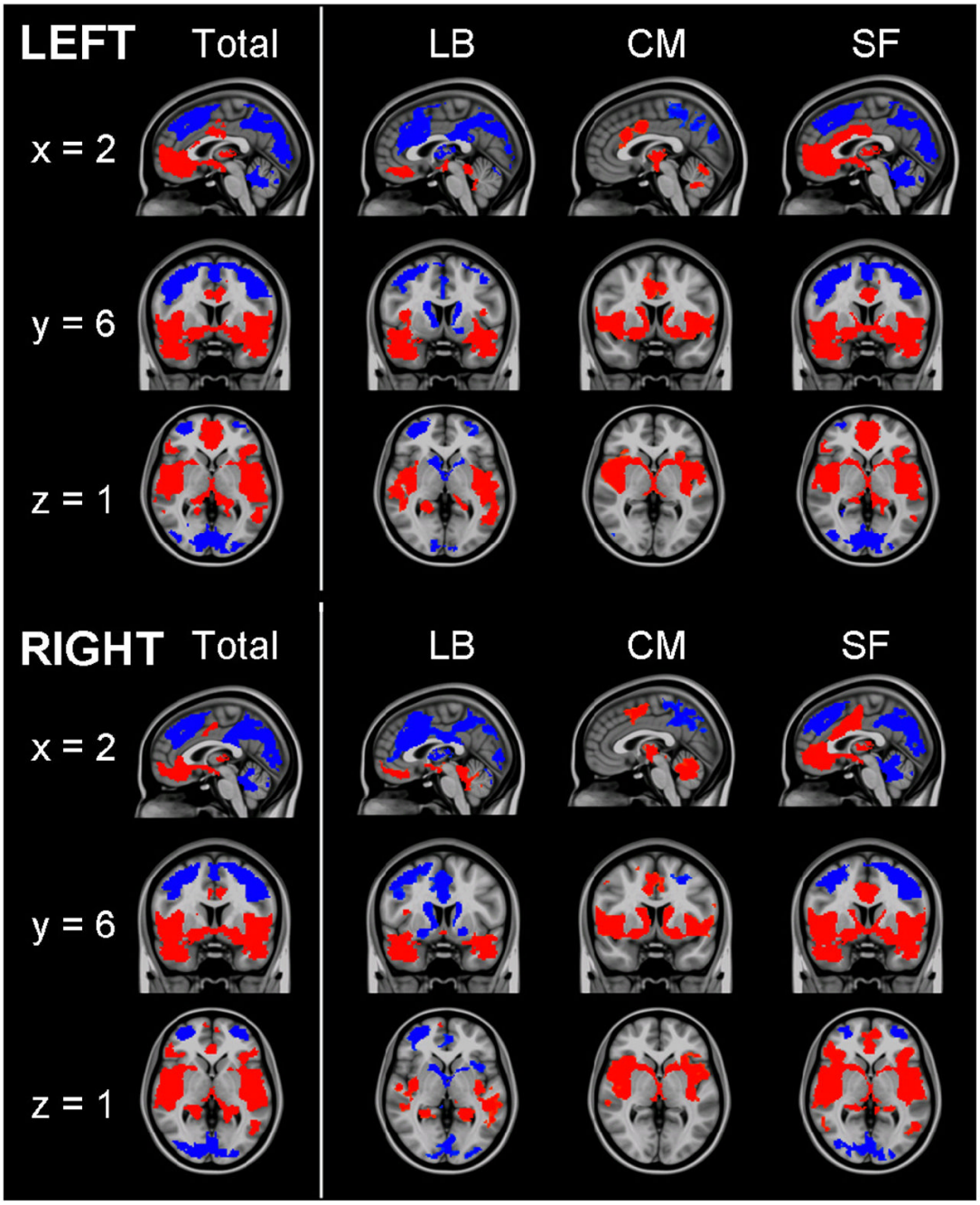

Figure 2.
Functional connectivity of amygdala regions of interest. Patterns of significantly positive (red) and negative (blue) relationships for the total amygdala, laterobasal (LB), centromedial (CM) and superficial (SF) subdivisions. Sagittal (x = 2), coronal (y = 6), and axial (z = 1) views are presented. (MNI standard space; radiological convention; Z > 2.3; cluster significance: $p < 0.05$, corrected).

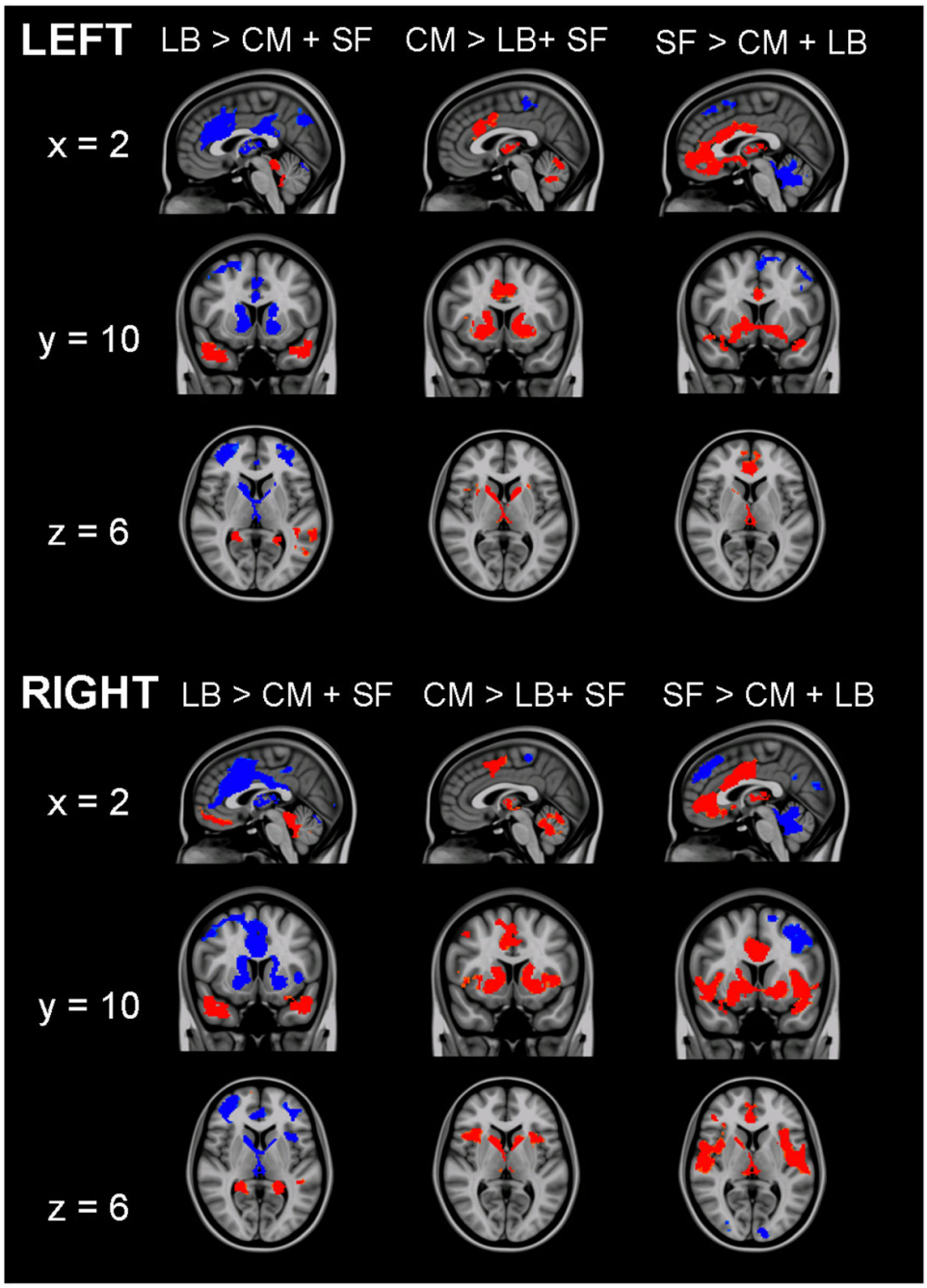

Figure 3.
Direct comparisons of the functional connectivity of each subdivision with the other two subdivisions. Red indicates regions in which activity is significantly more positively predicted by spontaneous activity in target subdivision than by the other two subdivisions. Blue indicates regions in which activity is significantly more negatively predicted by spontaneous activity in the target subdivision than by the other two subdivisions. Sagittal (x = 2), coronal (y = 10), and axial (z = 6) views are presented. (MNI standard space; radiological convention; Z > 2.3; cluster significance: $p < 0.05$, corrected).

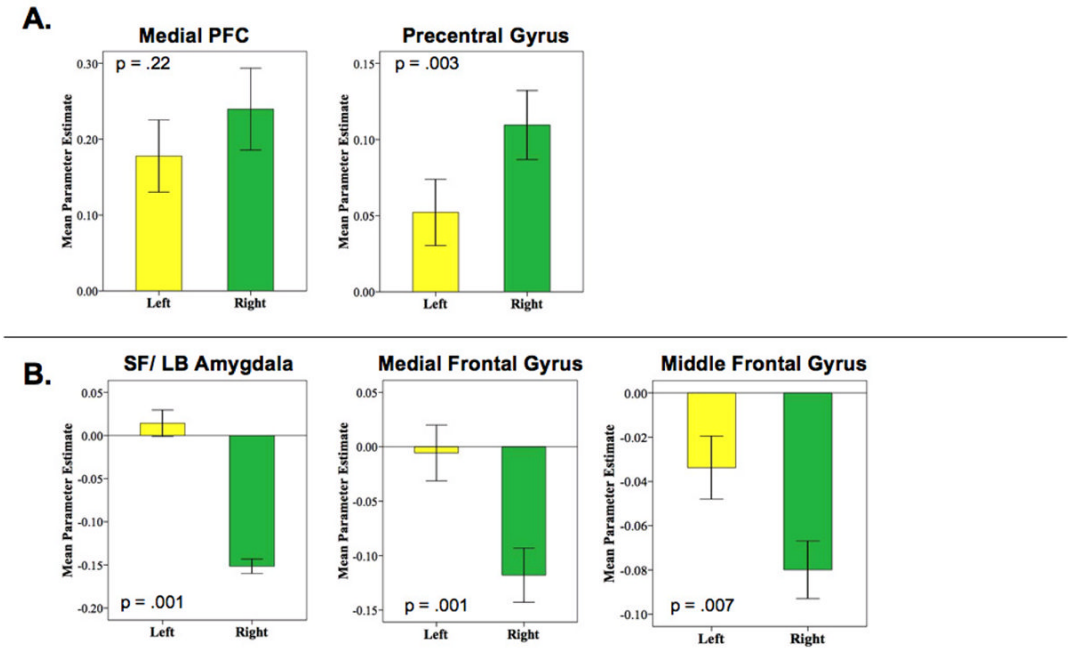

Figure 4.

Hemispheric comparisons of functional connectivity. Mean parameter estimates represent the strength of FC between regions. (A) Hemispheric comparisons of the functional connectivity of the laterobasal subdivision of the amygdala with medial prefrontal cortex (PFC) and precentral gyrus. (B) Hemispheric comparisons of the functional connectivity of the centromedial subdivision of the amygdala with the SF and LB subdivisions, middle frontal gyrus, and medial frontal gyrus.

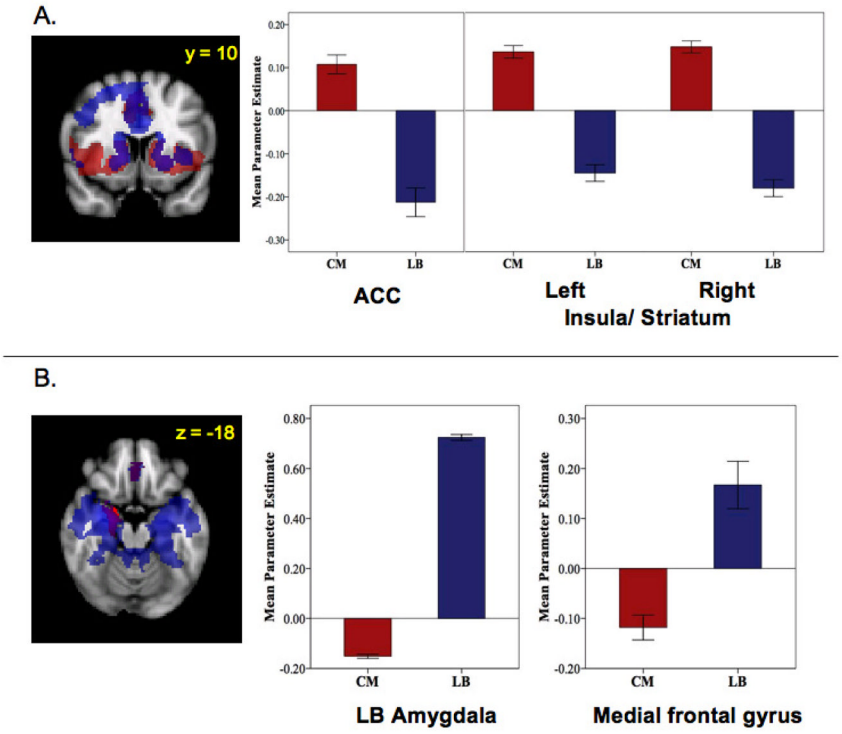

Figure 5.

Regions showing opposing patterns of functional connectivity for LB and CM amygdala subdivisions in the right hemisphere (MNI standard space; radiological convention; $Z > 2.3$; cluster significance: $p < 0.05$, corrected). Mean parameter estimates represent the strength of FC between amygdala subdivision and region indicated. (A) Regions positively predicted by activity in the centromedial (CM) subdivision (red) and negatively predicted by activity in the laterobasal (LB) subdivision (blue) and their overlap (purple). ACC: anterior cingulate cortex. (B) Regions negatively predicted by activity in the centromedial (CM) subdivision (red) and positively predicted by activity in the laterobasal (LB) subdivision (blue) and their overlap (purple).

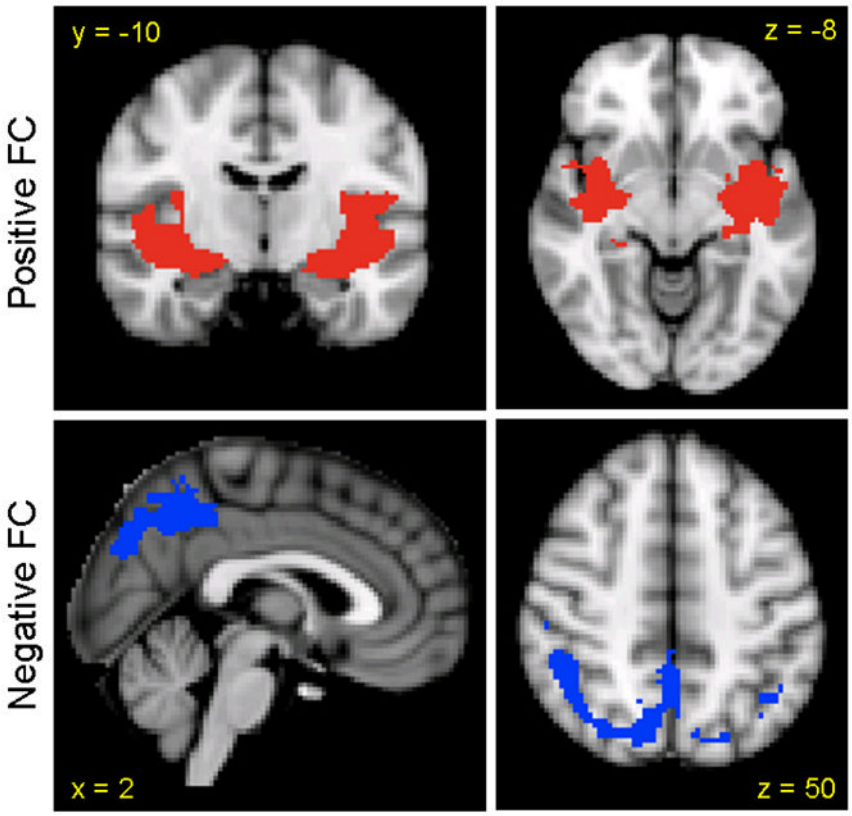

Figure 6.
Regions of convergence among amygdala subdivisions. Regions of positive functional connectivity are indicated in red and regions of negative functional connectivity are indicated in blue (MNI standard space; radiological convention; $Z > 2.3$; cluster significance: $p < 0.05$, corrected).

Table 1

Right Total Amygdala Functional Connectivity

Structure	BA	Cluster size	x[a]	y[a]	z[a]	Z Score[b]
Positive						
Cingulate gyrus (L)		2061	−8	−10	36	4.77
Cingulate gyrus (R)	31		14	−22	42	4.45
Laterobasal amygdala (R)		28844	28	−4	−22	11.8
Laterobasal amygdala (L)			−26	−10	−14	11.11
Superior temporal gyrus (R)	38		34	12	−30	9.66
	41		52	−30	16	4.85
Superior temporal gyrus (L)	38		−34	10	−30	8.68
			−60	−26	10	6.10
			−52	−2	−8	8.12
			−42	−44	18	4.26
Middle temporal gyrus (L)	21		−50	−18	−20	4.94
Inferior temporal gyrus (L)	19		−44	−54	−4	3.74
Fusiform gyrus (L)	20		−36	−42	−20	6.39
Fusiform gyrus (R)	20		38	−38	−18	5.77
Hippocampus (L)			−24	−38	−2	6.23
Caudate (R)			10	6	−6	8.03
Insula (R)			50	0	−6	7.90
			38	−16	2	7.64
Insula (L)			−36	−20	6	6.94
			−34	0	10	6.81
			−30	22	8	3.31
Anterior cingulate cortex (R)			2	42	−16	7.19
			0	24	−6	5.54
Inferior frontal gyrus (L)	47		−36	30	−14	6.50
Thalamus (R)			8	−24	4	5.10
Precentral gyrus (R)	6		52	−4	22	3.64
Brainstem/Pons (R)			14	−30	−26	4.66

Structure	BA	Cluster size	x[a]	y[a]	z[a]	Z Score[b]
Cerebellum (R)			6	−42	−8	4.56
Negative						
Cerebellum		1282	0	−44	−22	4.53
Cerebellum (L)			−10	−80	−24	4.16
			−30	−56	−30	3.65
Middle frontal gyrus (R)	8	13078	42	24	32	8.52
			30	8	56	6.62
			38	38	18	5.77
	10		24	60	14	5.13
Middle frontal gyrus (L)	6		−46	10	40	7.10
	6		−42	26	26	6.63
Cingulate gyrus	6		0	22	42	7.15
Superior frontal gyrus (R)	8		24	42	36	6.74
Superior frontal gyrus (L)	6		−18	14	58	5.67
	8		−2	42	46	4.59
	10		−24	52	16	5.69
Precentral gyrus (L)	6		−30	−4	60	6.08
Parietal lobe (R)	40	15047	50	−42	48	7.63
Angular gyrus (L)			−50	−56	38	6.69
Precuneus (L)	7		−6	−70	38	6.19
	7		−20	−68	54	4.88
Precuneus (R)	19		36	−64	46	6.34
	7		14	−72	40	5.91
Precuneus	31		0	−46	44	6.60
Cerebellum (R)			12	−78	−18	6.53
			30	−70	−22	4.65
Occipital lobe (L)	17		−8	−90	6	4.28
			−30	−88	16	5.30

Structure	BA	Cluster size	x[a]	y[a]	z[a]	Z Score[b]
Occipital lobe (R)			42	−76	10	3.65
Lingual gyrus (R)	18		2	−72	6	4.06
Superior parietal lobe (R)	7		32	−44	64	3.77
Inferior parietal lobe (L)	40		−42	−34	42	3.41

List of brain regions showing a significant positive or negative relationship with the right total amygdala (Z > 2.3; cluster significance: p < 0.05, corrected). For clusters with more than one peak, local maxima are listed. Cluster size in voxels. Coordinates are in standard MNI space. BA = Brodmann Area.

[a]Coordinates indicate location of maximum Z-scores for clusters or location of local maxima.

[b]Z Score: Maximum Z score of cluster or Z statistic of local maxima.

Table 2

Left Total Amygdala Functional Connectivity

Structure	BA	Cluster Size	x[a]	y[a]	z[a]	Z Score[b]
Positive						
Precentral gyrus (R)		1049	14	−24	50	4.6
Cingulate gyrus (R)	24		8	−8	36	4.26
Amygdala (L)		22843	−20	−4	−18	14.2
Hippocampus (R)			22	−12	−20	12.17
Superior temporal gyrus (R)	38		30	8	−30	9.93
	47		46	14	−18	5.94
	41		52	−30	14	3.27
	21		56	−4	−16	7.58
Superior temporal gyrus (L)	38		−40	16	−26	7.83
	22		−48	−4	−6	7.55
			−58	−32	10	4.97
Globus pallidus			10	4	−6	8.30
Medial frontal gyrus (R)	11		4	40	−18	8.14
Medial frontal gyrus (L)	9		−4	58	12	4.36
Fusiform gyrus (L)			−36	−12	−30	8.09
	20		−36	−42	−22	7.99
Fusiform gyrus (R)	20		36	−38	−18	4.98
Inferior frontal gyrus (L)	47		−34	32	−14	7.74
Inferior frontal gyrus (R)			48	34	−8	3.88
Middle temporal gyrus (L)			−50	−54	2	3.99
Insula (L)			−34	−18	8	6.66
Insula (R)			34	−20	4	6.25
			50	−4	8	5.63
Thalamus (R)			2	−16	6	5.82
Cingulate gyrus (L)	24		−2	32	0	5.43
Brainstem (L)			−8	−32	−4	5.03
Brainstem (R)			12	−32	−22	4.95

Structure	BA	Cluster Size	x[a]	y[a]	z[a]	Z Score[b]
Negative						
Middle frontal gyrus (R)		30505	42	20	42	8.58
Middle frontal gyrus (L)	9		−44	22	32	7.15
	6		−16	4	64	3.53
	10		−40	42	18	3.29
	10		−26	58	4	4.06
	10		28	58	2	5.65
Superior frontal gyrus (R)	6		28	6	58	7.66
	6		0	18	50	7.18
	6		8	2	66	4.26
	10		26	52	22	7.02
			14	42	42	3.96
Superior frontal gyrus (L)	9		−22	44	28	5.36
Precentral gyrus (L)	6		−46	4	46	6.07
Precentral gyrus (R)	9		48	4	24	3.72
Cingulate gyrus (R)	32		12	26	28	5.59
Angular gyrus (R)			48	−56	40	7.94
Angular gyrus (L)			−50	−60	38	6.66
Precuneus (R)	7		10	−76	44	7.87
	7		2	−52	44	6.50
Precuneus (L)	7		−8	−66	56	5.11
Cuneus (R)	18		10	−86	26	6.30
Cerebellum			0	−46	−22	4.89
Cerebellum (R)			10	−78	−18	5.84
			34	−56	−30	3.99
Cerebellum (L)			−12	−78	−22	4.78
			−30	−56	−30	4.16
Lingual gyrus (L)	17		−6	−92	6	5.42
Lingual gyrus (R)			12	−82	6	4.99
Inferior parietal lobe (R)	40		56	−28	46	5.05

Structure	BA	Cluster Size	x[a]	y[a]	z[a]	Z Score[b]
	40		36	−44	62	4.86
Inferior parietal lobe (L)	40		−42	−34	42	3.95
Superior parietal lobe (R)	7		20	−60	62	3.61
Occipital cortex (L)			−28	−88	16	6.07
Occipital cortex (R)			30	−78	18	5.34
	37		48	−72	8	4.29

List of brain regions showing a significant positive or negative relationship with the left total amygdala (Z > 2.3; cluster significance: p < 0.05, corrected). For clusters with more than one peak, local maxima are listed. Cluster size in voxels. Coordinates are in standard MNI space. BA = Brodmann Area.

[a]Coordinates indicate location of maximum Z-scores for clusters or location of local maxima.

[b]Z Score: Maximum Z score of cluster or Z statistic of local maxima.

Table 3

Right Laterobasal Functional Connectivity

Structure	BA	Cluster Size	x[a]	y[a]	z[a]	Z Score[b]
Positive						
Postcentral gyrus (R)	3	406	18	−36	66	4.00
Medial frontal gyrus (R)	11	410	4	40	−18	5.21
Superior frontal gyrus (L)	10		−6	56	−10	3.18
Precuneus (L)	7	433	−16	−42	60	4.01
Precentral gyrus (L)	4		−18	−20	64	3.59
Laterobasal amygdala (R)		12866	28	−2	−26	16.2
Hippocampus (L)			−26	−8	−24	10.85
			−22	−40	0	5.77
Parahippocampal gyrus (R)			32	−34	−10	4.85
Superior temporal gyrus (R)	38		42	10	−34	8.63
	21		52	0	−18	7.12
			44	−40	14	3.55
Superior temporal gyrus (L)	38		−38	14	−28	7.97
	13		−42	−46	20	4.19
	21		−48	−32	0	4.18
Fusiform gyrus (L)	20		−34	−42	−18	6.05
	37		−42	−64	−12	3.35
Cerebellum (R)			8	−44	−10	4.25
Brainstem/Pons (R)			18	−34	−32	5.87
Brainstem/Pons (L)			−10	−36	−26	5.54
Putamen (R)			34	−6	8	4.56
Insula (L)			−36	−6	−2	4.01
	13		−34	−16	18	3.38
Negative						

Structure	BA	Cluster Size	x[a]	y[a]	z[a]	Z Score[b]
Middle frontal gyrus (L)		1292	−42	32	26	5.21
Superior frontal gyrus (L)			−28	46	12	4.72
Cerebellum (R)		2338	26	−72	−20	5.81
Cerebellum (L)			−32	−72	−22	5.81
			−6	−78	−22	4.75
Middle occipital gyrus (L)	19		−36	−86	6	3.96
Lingual gyrus (L)			−4	−68	−2	3.16
Superficial Amygdala (R)		13791	20	−2	−14	8.66
Cingulate gyrus (R)	32		6	24	28	7.15
	31		2	−38	46	4.31
Cingulate gyrus (L)	32		−2	40	8	4.41
Middle frontal gyrus (R)	10		36	50	16	6.77
	9		36	36	32	6.14
	6		44	6	48	4.73
	6		24	8	58	5.73
Superior frontal gyrus (R)	10		24	50	−8	3.21
Medial frontal gyrus (R)			2	8	50	5.88
Thalamus			8	0	6	6.65
Insula (L)			−38	14	−2	5.13
Insula (R)			48	16	−6	4.63
			30	22	2	3.27
Precuneus (L)	7		−6	−74	38	4.80
	7		−4	−60	60	3.78
Inferior parietal lobe (R)	40		54	−38	48	5.51
	40		36	−46	62	3.41
Superior parietal lobe (R)	7		30	−68	50	3.54

List of brain regions showing a significant positive or negative relationship with the right laterobasal subdivision of the amygdala ($Z > 2.3$; cluster significance: $p < 0.05$, corrected). For clusters with more than one peak, local maxima are listed. Cluster size in voxels. Coordinates are in standard MNI space. BA = Brodmann Area.

[a]Coordinates indicate location of maximum Z-scores for clusters or location of local maxima.

[b] Z Score: Maximum Z score of cluster or Z statistic of local maxima.

Table 4

Left Laterobasal Functional Connectivity

Structure	BA	Cluster Size	x[a]	y[a]	z[a]	Z Score[b]
Positive						
Laterobasal amygdala		16218	−24	−6	−24	16.0
Laterobasal amygdala			22	−8	−22	10.64
Parahippocampal gyrus (L)			−28	−26	−18	8.80
	30		−20	−50	8	3.22
Parahippocampal gyrus (R)			18	−46	4	3.99
Superior temporal gyrus (R)	38		38	12	−32	8.96
			60	−34	10	3.87
Superior temporal gyrus (L)	13		−54	−40	22	5.21
Middle temporal gyrus (L)	37		−54	−60	2	3.82
Insula (R)			48	−14	−8	6.63
			36	−18	10	4.68
			32	12	0	3.51
Fusiform gyrus (R)	20		34	−40	−20	4.86
Fusiform gyrus (L)			−30	−58	−8	3.61
Thalamus (L)			−14	−30	2	4.52
Brainstem (R)			4	−38	−8	4.49
			16	−34	−30	4.45
Brainstem (L)			−18	−40	−32	4.39
Negative						
Parietal lobe (L)	40	888	−44	−60	46	4.49
Precuneus (L)	19		−30	−78	40	3.33
Globus pallidus (L)		1855	−16	−2	−12	5.84
Caudate (L)			−18	6	14	5.63
Caudate (R)			18	12	14	5.06
Thalamus (R)			2	−8	8	5.26

Structure	BA	Cluster Size	x[a]	y[a]	z[a]	Z Score[b]
Posterior cingulate	23	6140	4	−28	26	5.94
Cingulate gyrus	31		0	−40	44	4.52
Precuneus (L)	7		−6	−72	36	5.81
Precuneus (R)	7		14	−62	34	4.42
	19		30	−72	48	4.73
	7		2	−56	58	3.88
Cerebellum			0	−70	−12	3.66
Cerebellum (R)			22	−72	−18	5.73
			36	−52	−30	4.19
Cerebellum (L)			−22	−74	−24	5.40
			−36	−54	−30	4.17
Parietal lobe (R)			48	−56	42	5.67
	40		50	−36	52	4.58
Lingual gyrus			8	−90	−4	4.62
Cingulate gyrus	32	8871	0	20	40	7.60
Middle frontal gyrus (R)	9		38	20	40	6.86
	9		32	38	32	5.59
	6		32	6	56	6.45
			34	50	16	5.16
Middle frontal gyrus (L)			−38	26	38	4.80
	10		−24	58	6	4.72
			−38	36	18	3.89
	6		−38	8	48	3.52
Anterior cingulate (R)	24		6	30	20	5.68
	32		4	44	0	3.44
Medial frontal gyrus	6		0	6	64	3.60
Medial frontal gyrus (L)	9		−12	42	26	3.22
Superior frontal gyrus (R)			20	62	6	3.27
Precentral gyrus (L)	6		−32	−10	60	3.95

List of brain regions showing a significant positive or negative relationship with the left laterobasal amygdala (Z > 2.3; cluster significance: p < 0.05, corrected). For clusters with more than one peak, local maxima are listed. Cluster size in voxels. Coordinates are in standard MNI space. BA = Brodmann Area.

[a] Coordinates indicate location of maximum Z-scores for clusters or location of local maxima.

[b] Z Score: Maximum Z score of cluster or Z statistic of local maxima.

Table 5

Right Centromedial Functional Connectivity

Structure	BA	Cluster Size	x[a]	y[a]	z[a]	Z Score[b]
Cingulate gyrus (R)	24	1249	8	8	34	3.96
Cingulate gyrus (L)	24		−10	−12	40	3.28
Medial frontal gyrus (R)	6		8	−2	52	3.85
Cerebellum (R)		3043	12	−64	−20	5.83
			20	−38	−26	4.35
Cerebellum (L)			−20	−58	−22	7.27
			−2	−48	−22	4.12
Globus pallidus (R)		6611	26	−8	−8	18.82
Putamen (R)			30	10	2	6.31
Insula (R)	13		50	6	−4	5.48
	13		34	−14	18	4.03
	13		46	−20	2	5.26
Precentral gyrus (R)	6		60	0	14	5.14
	6		56	−4	34	4.06
Inferior parietal lobe (R)	40		60	−38	26	5.05
Putamen (L)		5533	−30	−10	−4	9.88
Caudate (L)			−14	0	12	6.22
Thalamus (L)			−4	−22	2	4.73
Insula (L)			−38	10	0	5.45
	13		−42	−20	10	5.01
Superior temporal lobe (L)	13		−56	−44	18	5.38
Precentral gyrus (L)	6		−58	2	22	3.33
			−40	−20	36	3.70
Inferior frontal gyrus (L)	45		−50	24	12	3.23
Negative						

Structure	BA	Cluster Size	x[a]	y[a]	z[a]	Z Score[b]
Parahippocampal Gyrus (R)	28	418	20	−4	−16	11.56
Anterior cingulate	10	446	0	52	−8	4.65
Medial frontal gyrus	11		0	34	−18	3.06
Middle frontal gyrus (L)	8	1136	−24	18	46	4.61
	6		−22	−2	60	3.48
Precentral gyrus (L)	9		−44	22	34	3.45
Superior frontal gyrus (L)	9		−18	38	30	3.68
			−12	60	12	3.12
Precuneus (R)	7	7858	8	−68	54	5.45
	7		2	−46	50	4.33
	31		6	−68	28	3.95
Precuneus (L)	7		−20	−66	56	3.91
Posterior cingulate (R)	30		20	−54	14	3.43
Posterior cingulate (L)	30		−8	−48	20	3.37
Occipital lobe (R)			42	−66	16	4.03
Occipital lobe (L)	18		−22	−86	24	4.37
Parietal lobe (R)	19		32	−74	36	4.36
Parietal lobe (L)	39		−42	−68	38	3.97
Superior parietal lobe (R)	7		32	−48	62	3.90
Supramarginal gyrus (R)	40		46	−34	36	3.67
Paracentral lobule (R)	5		12	−40	68	3.62

List of brain regions showing a significant positive or negative relationship with the right centromedial subdivision of the amygdala ($Z > 2.3$; cluster significance: $p < 0.05$, corrected). For clusters with more than one peak, local maxima are listed. Cluster size in voxels. Coordinates are in standard MNI space. BA = Brodmann Area.

[a] Coordinates indicate location of maximum Z-scores for clusters or location of local maxima.

[b] Z Score: Maximum Z score of cluster or Z statistic of local maxima.

Table 6

Left Centromedial Functional Connectivity

Structure	BA	Cluster Size	x[a]	y[a]	z[a]	Z Score[b]
Positive						
Cerebellum (R)		1368	22	−64	−20	4.82
			2	−64	−8	3.75
Cerebellum (L)			−16	−62	−20	5.31
Cerebellum			0	−56	−32	3.68
Cingulate gyrus (L)	24	1453	−4	22	26	5.29
	24		−6	4	38	4.58
Globus pallidus (L)		12382	−24	−8	−8	18.86
Putamen (R)			24	6	−4	8.71
			34	−20	−2	6.37
Caudate (R)			18	−8	20	4.38
Caudate (L)			−14	0	12	6.86
Insula (L)	13		−38	10	−4	5.93
	13		−50	−38	20	4.74
Precentral gyrus (R)	44		48	4	4	5.47
	6		56	−4	32	3.33
Precentral gyrus (L)	22		−56	−6	4	5.67
Thalamus (R)			2	−12	6	5.22
Inferior frontal gyrus (R)	47		40	26	−4	4.35
Inferior frontal gyrus (L)	13		−28	28	−10	5.03
	45		−52	22	6	3.50
Inferior parietal lobule (R)	40		54	−28	22	4.92
Brainstem (R)			10	−8	−12	3.55
Brainstem (L)			−16	−28	−8	4.49
Negative						
Precuneus (R)	7	10183	26	−68	46	6.05

Structure	BA	Cluster Size	x[a]	y[a]	z[a]	Z Score[b]
	7		4	−62	46	4.53
	7		2	−42	52	4.17
Precuneus (L)	7		−24	−66	34	4.29
Middle occipital gyrus (L)	18		−22	−88	22	5.93
Cuneus (R)	18		20	−88	26	3.43
	18		2	−78	28	5.27
Inferior parietal lobule (R)	40		44	−40	52	4.57
Postcentral gyrus (R)	7		10	−46	70	3.87
Paracentral lobule (R)	6		10	−24	68	3.68

List of brain regions showing a significant positive or negative relationship with the left centromedial amygdala (Z > 2.3; cluster significance: p < 0.05, corrected). For clusters with more than one peak, local maxima are listed. Cluster size in voxels. Coordinates are in standard MNI space. BA = Brodmann Area.

[a]Coordinates indicate location of maximum Z-scores for clusters or location of local maxima.

[b]Z Score: Maximum Z score of cluster or Z statistic of local maxima.

Table 7

Right Superficial Functional Connectivity

Structure	BA	Cluster Size	x[a]	y[a]	z[a]	Z Score[b]
Positive						
Cingulate gyrus (R)	24	2715	12	−6	42	5.24
			16	−30	46	5.19
Cingulate gyrus (L)	24		−4	6	32	5.45
Anterior cingulate (R)	33		2	20	16	4.38
Anterior cingulate (L)	10		−8	50	0	4.08
Precentral gyrus (R)	6		54	−2	24	3.90
Superficial amygdala (R)		24300	22	−4	−14	16.2
Parahippocampal gyrus (L)	28		−20	−2	−16	11.87
			−24	−24	−14	8.65
Uncus (R)			30	8	−28	8.09
Superior temporal gyrus (L)	42		−54	−30	14	6.92
	38		−32	14	−32	6.61
Middle temporal gyrus (R)	37		56	−56	−2	3.79
Insula (R)	13		38	0	2	8.94
	13		38	−20	4	8.11
Insula (L)	13		−38	−8	−2	8.88
	13		−32	−26	14	5.05
	13		−30	20	8	4.80
Thalamus			0	−12	6	6.69
Caudate (R)			18	0	16	5.71
Inferior frontal gyrus (R)	47		34	30	−14	7.68
	46		46	40	0	5.47
Inferior frontal gyrus (L)	47		−34	32	−12	6.79
Frontal medial gyrus (R)	11		2	40	−18	7.15
Anterior Cingulate (L)	24		−2	22	−8	5.38
Fusiform gyrus (R)	37		44	−46	−16	4.45
Fusiform gyrus (L)	37		−44	−56	−12	3.86

Structure	BA	Cluster Size	x[a]	y[a]	z[a]	Z Score[b]
Cerebellum (L)			−34	−42	−24	5.78
			−18	−60	−18	3.27
Negative						
Cerebellum		2015	0	−44	−22	5.70
Cerebellum (R)			12	−78	−20	4.78
			44	−64	−30	3.93
Cerebellum (L)			−6	−68	−28	3.40
Precentral gyrus (R)	9	11929	40	26	32	8.51
Middle frontal gyrus (R)	6		42	6	46	5.46
Middle frontal gyrus (L)	9		−44	18	40	7.56
	6		−30	−2	60	5.71
	10		−30	56	4	5.24
	9		−26	32	26	4.23
Superior frontal gyrus (R)	6		18	24	54	7.20
Superior frontal gyrus (L)	6		−16	22	56	6.73
Cingulate gyrus (L)	32		−2	30	36	6.83
Medial frontal gyrus	6		0	4	64	3.53
Medial frontal gyrus (R)	10		26	50	2	4.16
Angular gyrus (R)		14947	48	−56	38	7.07
Angular gyrus (L)			−50	−56	40	7.69
Precuneus (L)	7		−4	−62	44	6.39
	7		−20	−74	48	5.60
Cuneus (R)	18		14	−88	22	6.13
Middle occipital gyrus (R)	19		28	−82	8	4.54
Middle occipital gyrus (L)			−24	−90	20	6.09
Lingual gyrus (R)			4	−72	4	4.14
Lingual gyrus (L)	17		−6	−92	8	4.67
Cuneus	18		0	−76	30	4.92

Structure	BA	Cluster Size	x[a]	y[a]	z[a]	Z Score[b]
Cuneus (R)	19		30	−74	38	5.25
Inferior parietal lobule (L)	40		−44	−34	44	4.07
Postcentral gyrus (R)	2		52	−26	44	3.99

List of brain regions showing a significant positive or negative relationship with the right superficial subdivision of the amygdala (Z > 2.3; cluster significance: p < 0.05, corrected). For clusters with more than one peak, local maxima are listed. Cluster size in voxels. Coordinates are in standard MNI space. BA = Brodmann Area.

[a]Coordinates indicate location of maximum Z-scores for clusters or location of local maxima.

[b]Z Score: Maximum Z score of cluster or Z statistic of local maxima.

Table 8

Left Superficial Functional Connectivity

Structure	BA	Cluster Size	x[a]	y[a]	z[a]	Z Score[b]
Positive						
Superficial amygdala (R)	34	20590	18	−4	−18	11.18
Superficial amygdala (L)	28		−18	−4	−16	14.8
Superior temporal gyrus (R)	38		30	8	−30	8.08
	47		46	14	−18	5.40
Superior temporal gyrus (L)	22		−48	−4	−8	7.20
	38		−36	4	−22	7.00
Anterior cingulate (R)	32		6	40	−16	8.08
Inferior frontal gyrus (R)	47		28	30	−12	7.00
Inferior frontal gyrus (L)	47		−34	32	−14	7.24
Insula (R)	13		50	−2	−4	6.85
	13		36	6	10	4.33
Insula (L)	13		−36	−12	16	5.69
Claustrum (R)	13		38	−20	6	5.25
Thalamus (R)			2	−16	8	6.42
Putamen (L)			−18	10	8	4.06
Cingulate gyrus (L)	24		−6	0	30	4.03
Medial frontal gyrus (L)	9		−4	58	10	4.47
Middle temporal gyrus (R)	21		58	−16	−22	5.49
Parahippocampal gyrus (L)	36		−32	−32	−22	6.96
Fusiform gyrus (R)	20		38	−38	−18	4.30
Fusiform gyrus (L)	37		−48	−48	−16	4.10
Inferior temporal gyrus (L)			−52	−18	−26	3.95
Brainstem (R)			12	−32	−22	4.63
Negative						
Middle frontal gyrus (R)	9	28006	42	20	42	7.39
	10		28	58	0	4.03

Structure	BA	Cluster Size	x[a]	y[a]	z[a]	Z Score[b]
	6		28	6	56	6.70
Middle frontal gyrus (L)	6		−44	6	46	5.66
	9		−44	22	32	6.68
Medial frontal gyrus (R)	32		2	36	30	4.28
Medial frontal gyrus (L)	6		−4	0	62	4.37
Cingulate gyrus (R)	31		2	−38	44	3.35
Superior frontal gyrus	8		0	20	52	6.36
Superior frontal gyrus (R)	6		20	26	52	4.46
Superior frontal gyrus (L)	6		−20	12	58	5.10
	9		−22	44	28	4.10
Cuneus (R)	19		10	−76	42	6.24
Precuneus (L)	7		−10	−68	46	6.14
Postcentral gyrus (R)	3		56	−14	44	4.68
Postcentral gyrus (L)	1		−58	−22	40	3.82
Superior parietal lobule (R)	7		28	−60	50	5.54
Superior parietal lobule (L)	7		−32	−58	48	5.45
Inferior parietal lobule (R)	7		34	−44	62	4.77
Inferior parietal lobule (L)	40		−42	−36	42	4.28
Angular gyrus (R)			48	−56	40	7.36
Angular gyrus (L)			−50	−58	38	5.65
Middle occipital gyrus (R)	19		42	−76	12	5.22
Middle occipital gyrus (L)	19		−24	−86	22	5.26
Cerebellum (R)			26	−72	−12	4.84
Lingual gyrus (R)	18		14	−82	6	4.69
Lingual gyrus (L)	18		−18	−74	−6	3.82
	17		−4	−92	6	5.07
Cerebellum			0	−46	−22	5.73
Cerebellum (R)			10	−66	−28	4.45
Cerebellum (L)			−2	−68	6	3.54

List of brain regions showing a significant positive or negative relationship with the left superficial amygdala (Z > 2.3; cluster significance: $p < 0.05$, corrected). For clusters with more than one peak, local maxima are listed. Cluster size in voxels. Coordinates are in standard MNI space. BA = Brodmann Area.

[a] Coordinates indicate location of maximum Z-scores for clusters or location of local maxima.

[b] Z Score: Maximum Z score of cluster or Z statistic of local maxima.